Piezoelectric energy extraction from a cylinder undergoing vortex-induced vibration using internal resonance

Ritwik Ghoshal (ritwik@naval.iitkgp.ac.in)
Indian Institute of Technology Kharagpur https://orcid.org/0000-0001-9463-4896

Annette Joy
IIT KGP: Indian Institute of Technology Kharagpur

Vaibhav Joshi
Birla Institute of Technology & Science Pilani - K K Birla Goa Campus

Kumar Narendran
IIT Madras: Indian Institute of Technology Madras

Research Article

Keywords: Energy harvesting, Vortex-Induced Vibrations, Piezoelectric, Autoparametric System, Wake-oscillator models, Non-linear Rotative Gravity-Pendulum

Posted Date: April 21st, 2022

DOI: https://doi.org/10.21203/rs.3.rs-1552703/v1

Noname manuscript No.
(will be inserted by the editor)

Piezoelectric energy extraction from a cylinder undergoing vortex-induced vibration using internal resonance

Annette joy · Vaibhav Joshi · Kumar Narendran · Ritwik Ghoshal

the date of receipt and acceptance should be inserted later

Abstract A novel concept of utilizing the kinetic energy from ocean currents/wind by means of internal resonance is proposed to address the increasing global energy demand and generate clean and sustainable power. In this work, a non-linear rotative gravity pendulum is employed to autoparametrically excite the elastically mounted cylinder for a wide range of flow velocities. This concept is adopted to increase the oscillation amplitude of the cylinder due to vortex-induced vibration (VIV) in the de-synchronized region for energy harvesting. In this regard, a VIV-based energy harvesting device is proposed that consists of a cylinder with an attached pendulum, and energy is harvested with bottom-mounted piezoelectric transducers. The cylinder undergoes VIV when it is subjected to fluid flow and this excites the coupled fluid-multibody cylinder-pendulum system autoparametrically. In the de-synchronized region, when the vortex shedding frequency becomes two times the natural frequency of the pendulum, an internal resonance occurs.

A. Joy
Department of Ocean Engineering and Naval Architecture,
Indian Institute of Technology Kharagpur.

V. Joshi
Department of Mechanical Engineering,
Birla Institute of Technology & Science Pilani,
K K Birla Goa Campus, India-403726.

K. Narendran
Department of Ocean Engineering,
Indian Institute of Technology Madras,
Chennai, India-600036.

R. Ghoshal
Corresponding author
Department of Ocean Engineering and Naval Architecture,
Indian Institute of Technology Kharagpur,
West Bengal, India-721 302.
Tel.: +91-3222-283794
E-mail: ritwik@naval.iitkgp.ac.in

This helps in achieving a higher oscillation amplitude of the cylinder which does not happen otherwise. This study is focused on one degree-of-freedom (1-DoF) system where the cylinder is free to oscillate in the transverse direction of the fluid flow. The objective of this work is to numerically investigate the effect of a non-linear rotative gravity pendulum (NRGP) on the VIV characteristics and piezoelectric efficiency of the system. The numerical model is based on the wake-oscillator model coupled with the piezoelectric constitutive equation. The influence of the frequency ratio, mass ratio, torsional damping ratio and ratio of cylinder diameter to pendulum length of the NRGP device on response characteristics due to VIV is also investigated. A detailed comparative analysis in terms of electric tension and efficiency are performed numerically for flows with wide range of reduced velocities for the cylinder with and without NRGP. A comprehensive study on the implications of internal resonance between the pendulum and cylinder on generated electric tension is also reported.

Keywords Energy harvesting, · Vortex-Induced Vibrations, · Piezoelectric, Autoparametric System, · Wake-oscillator models, · Non-linear Rotative Gravity-Pendulum

1 Introduction

Vortex-induced vibrations (VIV) are one of the most common hydrodynamic phenomena with practical implications that can be observed when the structures are subjected to fluid flow. VIV has been studied in detail by a number of investigators such as Roshko [29], Griffin & Ramberg [18], Bearman [4]; in review articles of Williamson & Govardhan [38], Sarpkaya [30] and in books by Belvins [8], Sumer & Fredsøe [34]. Over the past few decades, many researchers have focused on different methods to harness the hydro-kinetic energy utilizing the vortex-induced motion of structures and convert it into electrical energy [5, 26]. The VIV of structural components can be converted to electrical power using electrostatic [22], electromagnetic [12] and piezoelectric generators [19] which can be used to power micro-electro-mechanical systems or for charging batteries in remote locations. These small-scale energy generating sources are useful in powering nearby electronic equipments and self-powered devices [21].

In recent years, there are numerous contributions focusing on efficient ways of extracting energy from VIV using piezoelectric transducers. These transducers have a unique capability of converting strain energy to electrical energy. The most common and easiest way to extract energy is by attaching the piezoelectric material on the flexible/elastically mounted structure. Truitt [35] devised a wind-based energy harvester, by fixing a Polyvinylidene fluoride (PVDF) piezoelectric material on a flag-like membrane, and obtained a maximum power of 1.5 mW. Song et al.[32] proposed a novel concept of energy harvesting utilizing VIV and wake-induced vibrations (WIV) of two tandem cylinders connected by piezoelectric membranes as cantilever, and recorded a maximum power output of 21 μW. Wang and Ko [37] harvested energy from a piezoelectric film fixed over the fluid flow channel. Barrero-Gil et al. [3] utilized galloping phenomena at higher flow velocities for harnessing energy. Numerical investigations were conducted by Mehmood et al. [25] by using electromechanical governing equations that couple the oscillation of

an elastically mounted cylinder fixed with piezoelectric material. They observed that there is a significant impact on synchronization width and amplitude due to load resistance. Franzini and Bunzel [15] carried out numerical investigation on the power output from cylinder mounted on piezoelectric harvesters subjected to VIV. In their study, two different configurations pertaining to 1- and 2-DoF VIV were studied. In both the configurations, power output and efficiency were higher when frequency of vortex shedding was near to the structural frequency, i.e., in the lock-in region. A maximum power output of 2.6 mW and 11 mW for 1- and 2-DoF was reported, respectively. Experimental investigations were conducted by Arionfard and Nishi [2] for a pivoted cylinder undergoing VIV for Reynolds number (Re) ranging from 2880 to 22300 and reported a maximum power output of 60 mW. In a subsequent experimental study, Nishi et al. [27] proposed an efficient way of extracting energy by placing a secondary cylinder between the generator and the primary cylinder exposed to VIV, which increased electric tension (voltage) upto 9 V. In a numerical investigation, Soti et al. [33] reported that attaching the cylinder to a magnet can give a maximum harvested dimensionless power upto 0.13 at $Re = 150$. A detailed discussion regarding the recent developments of various devices for piezoelectric energy harvesting can be found in review articles by Elahi et al. [11].

Recently the possibility of energy harvesting from parametrically forced pendulum has gained attention among many researchers [1, 23, 9]. Marszal [24] conducted both experimental and numerical methods to harvest energy from pendulum oscillations using a generator and reported that energy harvesting was more efficient for shorter pendulum length. Franzini et al. [16, 36] in a series of numerical investigations highlighted that parametric excitation can significantly influence energy harvesting. However, in most of the studies the effect of pendulum on the base structure was neglected. In the work by Das and Wahi [10], this effect was considered and it was concluded that the response was significantly influenced by pendulum rotation. Both vertical and horizontal configuration of pendulum was considered in their study, however no quantitative difference in terms of electrical power and efficiency were reported. To the best of authors' knowledge, the influence of attaching a non-linear rotative gravity pendulum on harvested electrical power and a detailed study on parametric/autoparametric resonance of this type of multibody system is yet to be explored.

Although energy extraction from ocean currents from VIV is not unfamiliar, in this work, the effect of attaching a non-linear rotative gravity pendulum (NRGP) on a VIV based energy harvesting device is studied. In this regard, the dynamics of a rigid cylinder with NRGP, mounted on an elastic support having piezoelectric harvesters, is studied numerically in 1-DoF VIV set-up. A non-linear wake-oscillator model is used for estimating the fluid load and a linear constitutive equation is employed for coupling solid-electric multibody system. The wake-oscillator model was first introduced by Birkhoff [6] and Birkhoff & Zarantonello [7]. The structural equation was added to the non-linear wake-oscillator equation in [20] with the help of Rayleigh equation followed by the work in [31] where a Van der Pol equation was employed. Fachinetti et al. [13] reported that acceleration coupling, is best suited for VIV. In this article, mathematical models for NRGP-VIV system coupled with piezoelectric harvester (PZH) device is presented and numerical simulations are performed to obtain oscillation amplitude, electric tension, and time-averaged electric power. Results are compared with existing numerical

models and experiments of similar devices. A detailed sensitivity study on internal resonance between cylinder-pendulum system and its influence on harvested electrical power is also presented.

Rest of the article is organized as follows: In Section 2, governing differential equations for 1-DoF VIV based on wake-oscillator model along with equation of motion of the autoparametric cylinder-pendulum system are discussed along with the problem definition. The numerical results obtained from the formulation are validated and compared with the literature in Section 3. The effect of the introduction of the NRGP on the amplitude response of the cylinder and piezoelectric harvesting capability are also discussed. A detailed parametric analysis of the coupled NRGP-PZH-VIV system is performed in Section 4. Finally, the concluding remarks on the efficacy of the proposed autoparametric oscillator based energy harvesting device are given in Section 5.

2 Coupled problem description and methodology

We begin with briefly describing the governing equations of the non-linear rotative gravity pendulum based vortex-induced vibration (NRGP-VIV) amplifier coupled with the piezoelectric harvester (PZH) in this section. The schematic of the NRGP-PZH-VIV system is shown in Fig. 1. The NRGP-PZH-VIV system consists of a circular cylinder of mass m_{s} and diameter D elastically mounted on a spring of stiffness k_y and damper with damping constant c_y. A pendulum of mass M is pivoted at the center of the cylinder with length L and a rotational damper of constant c_θ. A piezoelectric harvester is also connected to the base of the cylinder, having a resistance R_y, capacitance $C_{p,y}$, and electro-mechanical coupling parameter θ_y. When the cylinder is subjected to the incoming freestream velocity of U_∞, the cylinder oscillates due to VIV. It is envisaged that the multibody interaction of the cylinder with the pendulum may result in high amplitude oscillation in the desynchronized regime (internal resonance region), where energy can be harvested.

2.1 Governing equations and non-dimensionalization

The equations of motion of the cylinder-pendulum system can be written by considering the coupling between their motions. The kinetic and potential energy of the cylinder-pendulum system are calculated in order to obtain the Lagrangian of the system and subsequently the equations of motion are derived on the basis of Euler-Lagrange equation [14, 10]. The governing equations of the NRGP-PZH-VIV

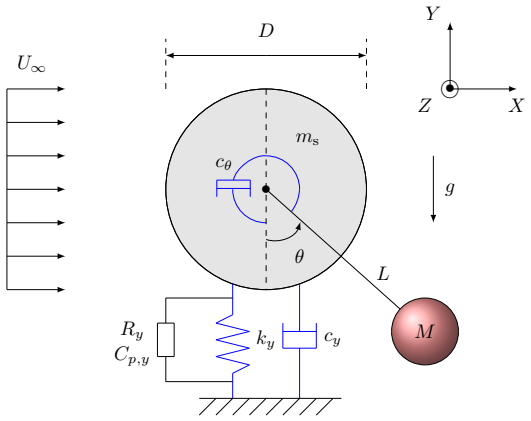

Fig. 1: A schematic description of the VIV based energy extraction device with a NRG pendulum.

system can be written as

$$(m_s + m_f + M)\frac{d^2Y}{dt^2} + c_y\frac{dY}{dt} + k_yY - \theta_yV_y + ML\left(\left\{\frac{d\theta}{dt}\right\}^2\cos\theta + \frac{d^2\theta}{dt^2}\sin\theta\right)$$
$$= \frac{1}{2}\rho U_\infty^2 DLC_{y,v}, \tag{1}$$

$$ML^2\frac{d^2\theta}{dt^2} + c_\theta\frac{d\theta}{dt} + ML\left(\frac{d^2Y}{dt^2} + g\right)\sin\theta = 0, \tag{2}$$

$$\frac{d^2q_y}{dt^2} + \varepsilon_y\omega_f(q_y^2 - 1)\frac{dq_y}{dt} + \omega_f^2 q_y = \frac{A_y}{D}\frac{d^2Y}{dt^2}, \tag{3}$$

$$C_{p,y}\frac{dV_y}{dt} + \frac{V_y}{R_y} + \theta_y\frac{dY}{dt} = 0, \tag{4}$$

where Eqs. (1) and (2) depict the coupled equations of motion for the cylinder and the pendulum, respectively. The displacement of the cylinder is denoted by $Y(t)$ and the angle of rotation of the pendulum is represented by $\theta(t)$. The added mass of the fluid is m_f and the acceleration due to gravity in the transverse direction is g. The fluid forces in the transverse direction on the right-hand side of Eq. (1) are represented by the coefficient $C_{y,v} = f(q_y)$. The wake variable q_y is solved using the wake-oscillator model [13] (Eq. (3)), where an acceleration coupling scheme is utilized on the right-hand side of the equation. The energy harvested from the piezoelectric system is evaluated by a constitutive equation that couples the piezoelectric energy generation with the movement of the cylinder [25], given in Eq. (4) where the voltage is denoted by V_y.

Choosing the time scale as $\tau = \omega_{n,y}t$ where $\omega_{n,y}$ is the natural frequency of the structural system in still water, given as

$$\omega_{n,y} = 2\pi f_{n,y} = \sqrt{\frac{k_y}{m_s + m_f + M}}, \tag{5}$$

and the length scale as $y = Y/D$, the coupled dynamics of NRGP-PZH-VIV system, given by Eqs. (1) - (4) can be written in non-dimensional form as

$$\ddot{y} + 2\zeta_y \dot{y} + y - v_y + \frac{\overline{m}}{l_d(1 + C_a/m^*)} \left(\dot{\theta}^2 \cos\theta + \ddot{\theta} \sin\theta \right) = \frac{U_r^2}{2\pi^3} \frac{1}{(m^* + C_a)} C_{y,v}, \quad (6)$$

$$\ddot{q_y} + \varepsilon_y St U_r (q_y^2 - 1)\dot{q_y} + (St U_r)^2 q_y = A_y \ddot{y}, \quad (7)$$

$$\ddot{\theta} + 2\zeta_\theta \dot{\theta} + (l_d \ddot{y} + \omega_r^2) \sin\theta = 0, \quad (8)$$

$$\dot{v_y} + \sigma_{2,y} v_y + \sigma_{1,y} \dot{y} = 0, \quad (9)$$

where $\dot{(\,)} = d(\,)/d\tau$ and $\ddot{(\,)} = d^2(\,)/d\tau^2$ and the dimensionless parameters are defined below:

$$\zeta_y = \frac{c_y}{2(m_\mathrm{s} + m_\mathrm{f} + M)\omega_{n,y}}, \qquad v_y = \frac{V_y \theta_y}{V_0}, \qquad \overline{m} = \frac{M}{M + m_\mathrm{s}},$$

$$C_a = \frac{m_\mathrm{f}}{m_\mathrm{d}}, \qquad m^* = \frac{m_\mathrm{s} + M}{m_\mathrm{d}}, \qquad l_d = \frac{D}{L},$$

$$U_r = \frac{U_\infty}{f_{n,y} D}, \qquad St = \frac{\omega_f D}{2\pi U_\infty}, \qquad \zeta_\theta = \frac{c_\theta}{2ML^2\omega_{n,y}},$$

$$\omega_r = \frac{\omega_{n,p}}{\omega_{n,y}}, \qquad \sigma_{1,y} = \frac{\theta_y^2}{C_{p,y}(m_\mathrm{s} + m_\mathrm{f} + M)\omega_{n,y}^2}, \qquad \sigma_{2,y} = \frac{1}{C_{p,y} R_y \omega_{n,y}}.$$

Here, the displaced mass of the fluid is denoted by $m_\mathrm{d} = (\pi \rho D^2 \widetilde{L})/4$, $\widetilde{L}$ being the span of the cylinder. The reference electric tension is represented by $V_0 = (m_\mathrm{s} + m_\mathrm{f} + M)\omega_{n,y}^2 D/\theta_y$. The natural frequency of the pendulum is denoted by $\omega_{n,p}$. Among the non-dimensional parameters, m^* represents the ratio of the combined mass of the cylinder and pendulum to that of the displaced fluid, whereas $\overline{m}$ denotes the ratio of the cylinder mass to the combined mass of the cylinder-pendulum system. Note that ω_r, $\overline{m}$, ζ_θ and l_d describe the coupling between the cylinder and the pendulum, which are crucial for studying the effect of internal resonance on the response of the coupled fluid multibody cylinder-pendulum system.

When the cylinder is considered to be stationary, the right-hand side of Eq. (7) is zero and thus, solving the equation leads to a limit-cycle periodic solution of wake variable amplitude $\widehat{q}_y = 2$. The force coefficient in the cross-flow direction ($C_{y,v}$) due to vortex shedding in Eq. (6) can be computed by resolving the fluid force as

$$C_{y,v} = \left(C_{L,v} - \frac{C_{D,v} 2\pi \dot{y}}{U_r} \right) \sqrt{1 + \left(\frac{2\pi \dot{y}}{U_r} \right)^2}, \quad (10)$$

where $C_{L,v} = (q_y/\widehat{q}_y)\widehat{C}_L^o$ is the oscillatory lift coefficient and $\widehat{C}_L^o = 0.3842$ is the lift coefficient obtained from the flow around a stationary cylinder [28]. The details of this derivation using the geometric relations can be found in [15]. The drag coefficient is represented by $C_{D,v} = 1.1856$.

Empirical parameters related to wake-oscillator model (ε_y and A_y) are considered from the work of Ogink and Metrikine [28], wherein two sets of parameters

were proposed, viz., for upper-branch ($U_r < 6.5$) and lower-branch ($U_r \geq 6.5$) as follows:

$$\varepsilon_y = \begin{cases} 0.05, \text{ for} & U_r < 6.5 \\ 0.7, \text{ for} & U_r \geq 6.5 \end{cases}, \qquad A_y = \begin{cases} 4, \text{ for} & U_r < 6.5 \\ 12, \text{ for} & U_r \geq 6.5 \end{cases}. \tag{11}$$

The upper- and lower-branches are associated with the higher and lower oscillation amplitudes, respectively. The upper branch represents the synchronized region where the natural frequency of the oscillating system matches with the vortex shedding frequency leading to resonance condition and thus, higher response amplitudes. Typically, the reduced velocity range of $U_r \in [5, 10]$ is observed in the synchronized region. On the other hand, the lower branch depicts the de-synchronized region where the natural frequency of the system is no more equal to the vortex shedding frequency resulting in absence of resonance and lower amplitudes.

The electric power generation due to the piezoelectric harvester is quantified by the electrical power $P_{el,y}$ and the harvesting efficiency $\eta_{el,y}$ given by [15]

$$P_{el,y} = \frac{V_y^2}{R_y}, \tag{12}$$

$$\eta_{el,y} = \frac{P_{el,y}}{(1/2)\rho U_\infty^3 D\widetilde{L}} = \frac{4\pi^4}{U_r^3}\frac{\sigma_{2,y}}{\sigma_{1,y}}(m^* + C_a)v_y^2, \tag{13}$$

where the expression for efficiency is obtained by making the electric power dimensionless with respect to the flux of fluid kinetic energy across the cylinder frontal area.

2.2 Problem description

In this work, the influence of the NRGP system on the VIV of a cylinder is studied, with a focus on the electrical power extraction using piezoelectric materials. In particular, a special attention is paid to the interaction between the coupled fluid-multibody-electrical system. The equations for this system (Eqs. (6)-(9)) are solved using fifth-order Runge–Kutta integration based on ordinary differential equation solver in MATLAB, with a fixed time step size of $\Delta t = 0.02$. The non-trivial initial conditions used in these simulations are $q_y(0) = 0.01$ and $\theta(0) = \pi/3$. The simulations are performed till a large non-dimensional time τ so that the initial transient effects are negligible. In order to understand the coupled multibody dynamics of the cylinder-NRG pendulum system subjected to VIV, four different models are considered, which are as follows:

- **Pure-VIV**: In the literature, Pure-VIV usually refers to a configuration wherein the spring mounted cylinder system is allowed to undergo VIV freely, without attaching any harvesters. Moreover, the NRG pendulum is also ignored in this case and therefore, to simulate Pure-VIV condition, $\sigma_{1,y} = \sigma_{2,y} = v_y = \overline{m} = 0$ in Eqs. (6)-(9).
- **VIV with Piezoelectric harvesters (PZH-VIV)**: In this case, piezoelectric harvesters are considered, however, the effect of NRG pendulum is not included. This is achieved by setting $\overline{m} = 0$ and $\theta = 0$ in the Eqs. (6)-(9), making it similar to the formulation given in [15].

Table 1: Non-dimensional parameters for the NRGP-PZH-VIV system

Parameter description	Symbol	Value
Linear damping ratio	ζ_y	0.0007
Mass ratio of cylinder-pendulum system	$\overline{m}$	0.3
Added mass coefficient	C_a	1
Mass ratio of cylinder-pendulum-fluid system	m^*	2.6
Ratio of cylinder diameter to pendulum length	l_d	0.1
Strouhal number	St	0.1932
Rotational/torsional damping ratio	ζ_θ	0.0011
Frequency ratio	ω_r	1.3
Dimensionless piezoelectric parameter 1	$\sigma_{1,y}$	0.35
Dimensionless piezoelectric parameter 2	$\sigma_{2,y}$	21.4
Initial angle of pendulum	θ_0	$\pi/3$

- **VIV with NRG pendulum (NRGP-VIV)**: Coupled multibody dynamics of the cylinder-pendulum system subjected to VIV, without including the piezoelectric effects are considered here. Therefore, $\sigma_{1,y} = \sigma_{2,y} = v_y = 0$ is substituted in Eqs. (6)-(9) and thereby making it similar to the expressions obtained in [10].
- **VIV with NRG pendulum with Piezoelectric harvesters (NRGP-PZH-VIV)**: In this case, the coupled fluid-multibody-electric system is solved to compute the efficiency of NRG pendulum which is parametrically excited due to VIV. However, since it is a coupled fluid-multibody system, NRGP also influences the cylinder motion, thereby causing fluctuation in fluid forces, which makes it an autoparametric system. Moreover, pendulum parameters are chosen in such a way that the frequency of NRGP is harmonic to the vortex shedding frequency and internal resonance occurs. The effect of internal resonance phenomena on the overall system response and the generated electrical power is the primary focus of this study. Therefore, Eqs. (6)-(9) are solved with the initial conditions stated above.

The parameters for the present study are listed in Table. 1. The mass ratio of cylinder-pendulum-fluid system ($m^* = 2.6$) and the structural damping ratio ($\zeta_y = 0.0007$) are selected from the available literature [17]. The added mass coefficient is taken as $C_a = 1$. The effects of the NRG pendulum are incorporated by considering the mass ratio of the cylinder-pendulum system $\overline{m} = 0.3$, ratio of cylinder diameter to the pendulum length $l_d = 0.1$, frequency ratio $\omega_r = 1.3$ and the torsional damping ratio of $\zeta_\theta = 0.0011$. The material parameters for the piezoelectric harvesters are chosen from the work Mehmood et al. [25]. Here, the numerical simulations are carried out for all the four models mentioned above with slightly wider range of Re, ranging from 1.4×10^3 to 2.75×10^4.

It should be noted that a sensitivity analysis is carried out with an aim to investigate the influence of the NRG pendulum parameters on the response of the hydro-elastic multibody system. In particular, the NRG pendulum parameters are chosen in such a way that it triggers an internal resonance. Therefore, the study focuses on the effect of internal resonance on overall response and its possible exploitation to extract more electrical power over a wide range of reduced velocities apart from the lock-in range. It is worth mentioning that the use of a wake-

oscillator model to predict the hydrodynamic loads allows for a wider investigation in the sensitivity analysis presented here.

3 Validation and comparative study

In this section, a study on the relative performance for all the four different models are presented. The results for the Pure-VIV case are validated with the experimental results of Franzini et al. [17,16] where the influence of pendulum and piezoelectric harvesters are absent. The variation in the oscillation amplitude of the cylinder, hydrodynamic forces and response frequency are observed and compared for the various models to understand the effect of the introduction of the NRGP on the response of the system. Furthermore, the energy harvesting capability is also compared for the scenarios when the piezoelectric harvester is incorporated, viz., PZH-VIV and NRGP-PZH-VIV.

The maximum non-dimensional oscillation amplitude ($y_{\max}$) of the cylinder for all the four different models are presented as a function of reduced velocity (U_r) in Fig. 2(a). In these calculations, the values of non-dimensional parameters $\omega_r = 1.3$, $\overline{m} = 0.3$, $l_d = 0.1$ and $\zeta_\theta = 0.0011$ are considered. The experimental results of Pure-VIV case from the work of Franzini [17] are also included in the plot for comparison. It can be observed that the response profile of Pure-VIV and PZH-VIV are identical for $U_r \in [0-4, 11-20]$. The PZH-VIV response for $U_r \in [4-11]$ is slightly lesser compared to the Pure-VIV case. Simulation results from Pure-VIV and PZH-VIV cases are in good agreement with the results presented in the work by Franzini [17] for asymptotic values of NRG pendulum parameters, and it validates the mathematical framework presented herein. For all the four models, a rise in oscillation amplitudes can be observed at $U_r = 4$ and it reaches a peak value at $U_r = 5.5$. This can be attributed to the frequency lock-in, i.e., the synchronization of the vortex shedding frequency with the structural frequency of the system. However, when a NRG pendulum is added to the system, an increase in the peak oscillation amplitude of the cylinder ($y_{\max}$) is observed at $U_r \geq 11$. This increase of $y_{\max}$ in the de-synchronized region is due to the internal resonance between the NRG pendulum and the elastically mounted cylinder system. A slight reduction in the oscillation amplitude for the system with piezoelectric harvesters is observed in the response profiles of PZH-VIV (compared to Pure-VIV) and NRGP-PZH-VIV (compared to NRGP-VIV) systems. This reduction can be attributed to the conversion of mechanical to electrical energy.

The in-line and cross-flow force coefficients can also be obtained from the non-dimensional equations, which are given as [36]

$$C_x = \sqrt{1 + \left(\frac{2\pi\dot{y}}{U_r}\right)^2}\left(C_{D,v} + \frac{2\pi}{U_r}\frac{\widehat{C}_L^o}{\widehat{q}_y}\dot{y}\right), \tag{14}$$

$$C_y = -\frac{2\pi^3}{U_r^2}C_a\ddot{y} + \sqrt{1 + \left(\frac{2\pi\dot{y}}{U_r}\right)^2}\left(\frac{\widehat{C}_L^o}{\widehat{q}_y}q_y - C_{D,v}\frac{2\pi}{U_r}\dot{y}\right). \tag{15}$$

The mean in-line force coefficient ($C_{x,\text{mean}}$) and root-mean-square (rms) cross-flow force coefficient ($C_{y,\text{rms}}$), for the considered models are also shown in Figs. 2(b) and (c) respectively, along with the available measurements of Pure-VIV in [17].

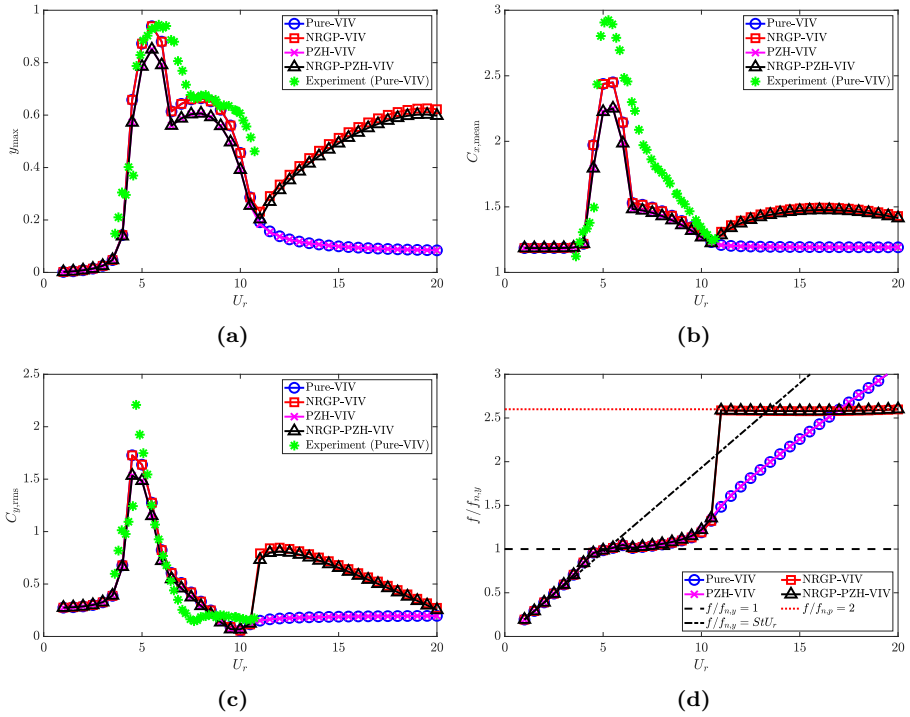

Fig. 2: Response characteristics of the system with U_r: (a) maximum non-dimensional oscillation amplitude ($y_{\max}$) of the cylinder, (b) mean in-line force coefficient $C_{x,\text{mean}}$, (c) root-mean-square cross-flow force coefficient $C_{y,\text{rms}}$, and (d) dominant frequency with respect to cylinder natural frequency $f/f_{n,y}$. For the NRGP cases, $\overline{m} = 0.3$, $l_d = 0.1$, $\omega_r = 1.3$ and $\zeta_\theta = 0.0011$.

The variation of $C_{x,\text{mean}}$ for NRGP-VIV is same as Pure-VIV until $U_r = 11$ (Fig. 2(b)). A jump is observed in the de-synchronized region which is maintained until $U_r = 20$. Similarly for $C_{y,\text{rms}}$ (Fig. 2(c)), the variation is similar for Pure-VIV and NRGP-VIV cases, till $U_r = 11$, after which a profound jump is observed and reaches maximum at $U_r = 12$. $C_{y,\text{rms}}$ decreases with further increase in U_r. This increase in the force coefficients in the de-synchronized region at $U_r \geq 11$ is associated with the occurrence of internal resonance. The peak values of the present analytical models are lower by about 16% and 22% compared to experimental values of $C_{x,\text{mean}}$ and $C_{y,\text{rms}}$, as shown in Figs. 2(b) and (c), respectively. Except the peak values, the trend of the models match with the experimental measurements satisfactorily.

Figure 2(d) presents the variation of the non-dimensional response frequency $f/f_{n,y}$ as a function of U_r. The frequency lock-in when the vortex shedding frequency equals the structural frequency, $f/f_{n,y} = 1$ is also shown in the figure. The lock-in is observed at $U_r = 4 - 10$. For Pure-VIV and PZH-VIV models, the dominant frequency follows the Strouhal law beyond the synchronized region. In case of NRGP models, with further increase in U_r there is a jump in the $f/f_{n,y}$ values

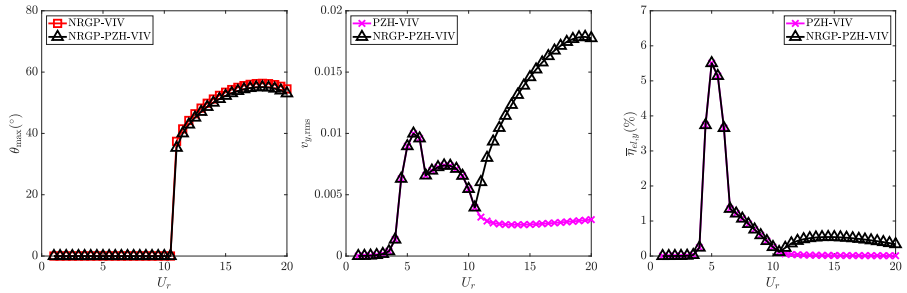

(a) **(b)** **(c)**

Fig. 3: Effect of the introduction of NRGP with U_r on: (a) maximum angular rotation of the pendulum $\theta_{\max}$ in degrees ($^\circ$), (b) electric tension $v_{y,\mathrm{rms}}$, and (c) energy harvesting efficiency $\overline{\eta}_{el,y}$. For the NRGP cases, $\overline{m} = 0.3$, $l_d = 0.1$, $\omega_r = 1.3$ and $\zeta_\theta = 0.0011$.

observed in the figure from 1.1 to 2.6 at $U_r \geq 11$. This jump is associated with the internal resonance due to the NRG pendulum, which increases the oscillation amplitude in the de-synchronized region, as shown in Fig. 2(a). Here, the resonance occurs when the vortex shedding frequency is two times the natural frequency of the pendulum ($f = 2f_{p,y}$), which can be observed in the plot. From $U_r \geq 11$, the frequency lock-in with $f_{n,p}$ continues till $U_r = 20$.

To understand the effect of NRGP on VIV, the oscillation of the pendulum in terms of angular position is presented in the Fig. 3(a) as a function of U_r. It can be observed that the pendulum oscillation is zero at the synchronized region and starts to oscillate only in the de-synchronized region ($U_r \geq 11$). The oscillation of the pendulum is associated with the internal resonance which occurs in the de-synchronized region. The electrical parameters such as non-dimensional electric tension and piezoelectric harvesting efficiency are associated with the oscillation amplitude of the cylinder and vary with U_r. Figures 3(b) and (c) present the piezoelectric harvesting capacity for electrical parameters such as rms of electric tension ($v_{y,\mathrm{rms}}$) and efficiency ($\overline{\eta}_{el,y}$) for U_r ranging from 1 to 20. The pattern of $v_{y,\mathrm{rms}}$ and $\overline{\eta}_{el,y}$ are similar for systems with and without NRGP till $U_r = 11$. The difference can be observed for $U_r > 11$. The $\overline{\eta}_{el,y}$ is 5.5% at $U_r = 5$, which is maximum. At the $U_r = 11$ to 20, the efficiency is around 0.6% for the NRGP system as shown in Fig. 3(c).

The time histories of the cylinder cross-flow displacement (y), angular oscillation of the pendulum and the frequency spectrum of the cylinder response y for all the four models at $U_r \in [4, 6, 12, 14]$ are shown in Figs. 4(Left), (Middle) and (Right), respectively. At $U_r = 4$, the amplitude of the cylinder for Pure-VIV and NRGP-VIV are similar. A slight reduction in amplitude for system with PZH is observed, as shown in Fig. 4(a-Left). The corresponding pendulum oscillation is zero and the frequency of the cylinder oscillation is close to unity, as shown in Fig. 4(a-Middle and Right). At the synchronization region, i.e., $U_r = 6$, a drastic increase in the amplitude of cylinder response is observed for all cases, however the response of Pure-VIV and NRGP-VIV is slightly larger compared to PZH systems, as shown in Fig. 4(b-Left). Similar to $U_r = 4$, the pendulum oscillation at

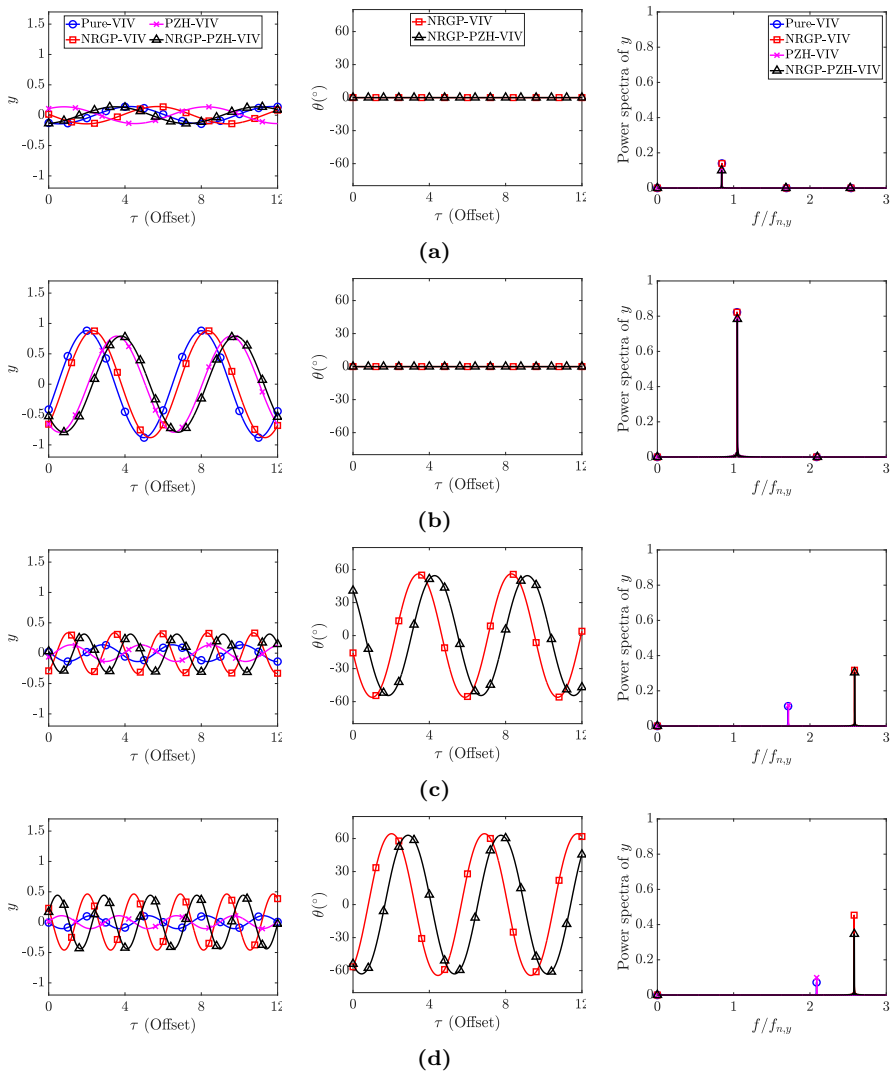

Fig. 4: Response amplitude of the cylinder y (left) and angular rotation of the pendulum $\theta(^\circ)$ (middle) and the power spectrum of the amplitude response y (right) for various reduced velocity U_r: (a) 4, (b) 6, (c) 12, and (d) 14. Note that the X-axis in the time history plots has been offset for clarity.

$U_r = 6$ is zero and the peak frequency is at the lock-in frequency as expected, i.e., $f/f_{n,y} = 1$, as shown in Figs. 4(b-Middle, Right). With further increase in U_r, the system enters the de-synchronized region, where the cylinder oscillation amplitude reduces and an internal resonance is triggered by the pendulum oscillation. As shown in Fig. 4(c-Left), the cylinder oscillations are reduced compared to $U_r = 6$. However, the difference of the introduction of NRGP can be observed clearly as the oscillation amplitude for NRGP-VIV and NRGP-PZH-VIV models are higher

compared to non-pendulum models. The pendulum oscillation increases as shown in Fig. 4(c-Middle). The dominant frequency shifts to the higher frequency region, where the vortex shedding frequency is 2 times the pendulum natural frequency, i.e., $f/f_{n,p} = 2$ for the NRGP cases, as shown in Fig. 4(c-Right). Therefore, from the spectrum plots it is evident that the internal resonance helps in achieving higher oscillation amplitude at higher U_r, making the synchronization width more wider compared to the system without NRGP. Pure-VIV and PZH-VIV models follow the Strouhal law in the de-synchronized region. A similar observation can be made for $U_r = 14$ in Fig. 4(d) where increase in the cylinder oscillation amplitudes and pendulum oscillations are observed. Therefore, the introduction of NRGP increases the range of U_r where energy extraction can be possible.

4 Parametric study of the NRGP-PZH-VIV system

In the previous section, we investigated the effect of the introduction of the pendulum on the VIV response and its energy extraction. Here, we carry out parametric study to understand the effect of the coupled parameters of the cylinder-pendulum system on the response and piezoelectric harvesting capabilities. A range of frequency-ratio (ω_r), pendulum mass-ratio ($\overline{m}$), torsional damping-ratio (ζ_θ) and ratio of cylinder diameter to pendulum length (l_d) are considered to understand their effect on the NRGP-PZH-VIV system. Moreover, the generated electric tension and efficiency are computed and compared with the model without the NRG pendulum (PZH-VIV model).

4.1 Effect of frequency ratio (ω_r)

The frequency ratio ω_r depicts the ratio of the natural frequencies of the pendulum and the cylinder and is one of the crucial parameters to study the effect of the NRGP on the response of the cylinder in the de-synchronized region. Here, we consider a range of $\omega_r \in [0.5, 1, 1.3, 1.5]$, while all other parameters remain fixed, $\overline{m} = 0.3$, $l_d = 0.1$ and $\zeta_\theta = 0.0011$.

The cylinder and pendulum response characteristics for various ω_r is shown in Fig. 5. The result for PZH-VIV model is also shown for comparison. When the $\omega_r = 0.5$, the oscillation amplitude of the cylinder follows the pattern of PZH-VIV for all U_r, as shown in the Fig. 5(a). A small dip in the cylinder oscillation amplitude is observed at $U_r = 5$, which can be correlated to the maximum pendulum oscillation observed at the same U_r for $\omega_r = 0.5$ as shown in Fig. 5(b). The effect of internal resonance in the de-synchronized region is observed when $\omega_r \geq 1$. The jump in the oscillation amplitude occurs at $U_r = 9$, 11 and 12.5 for $\omega_r = 1$, 1.3 and 1.5, respectively. A quick drop in the amplitude is observed for $\omega_r = 1$ at $U_r = 17$ and the responses are similar to PZH-VIV thereafter, as shown in the figure. For $\omega_r = 1.3$ and 1.5, the oscillation amplitude are higher in the de-synchronized region. In fact, the amplitude values are higher for $\omega_r = 1.3$ compared to 1.5. The pendulum oscillations in the de-synchronized region begins at $U_r = 9$, 11 and 12.5, for $\omega_r = 1$, 1.3 and 1.5 similar to the cylinder oscillation jumps (Fig. 5(b)). Therefore, the onset of autoparametric excitation of the cylinder response gets

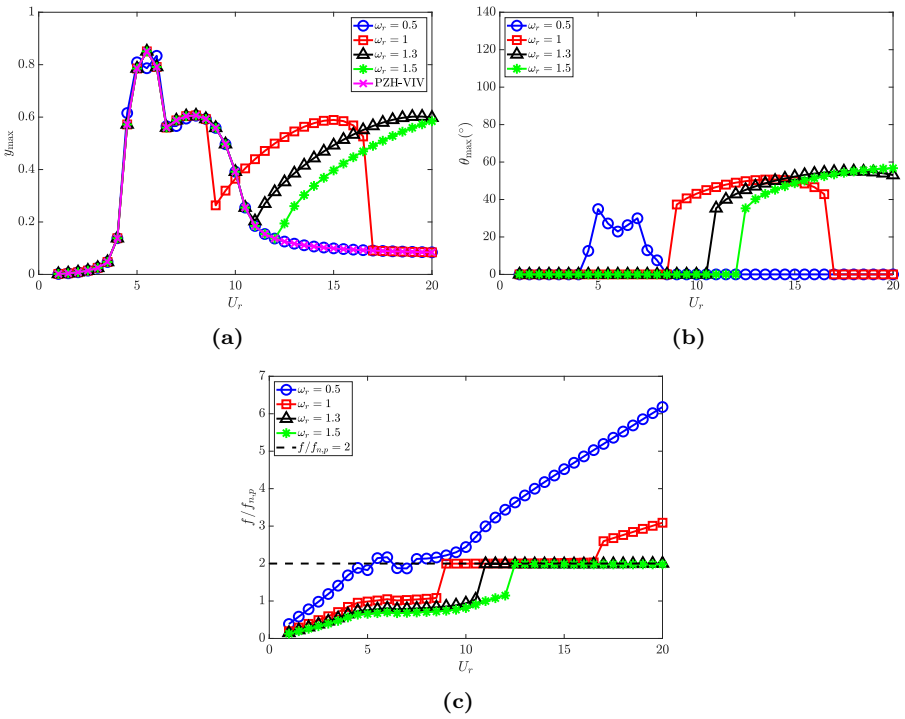

Fig. 5: Response characteristics of the system for various ω_r with U_r: (a) maximum non-dimensional oscillation amplitude ($y_{\max}$) of the cylinder, (b) maximum angular rotation of the pendulum $\theta_{\max}$ in degrees ($^\circ$) and (c) dominant frequency with respect to pendulum natural frequency $f/f_{n,p}$. Here, $\overline{m} = 0.3$, $l_d = 0.1$ and $\zeta_\theta = 0.0011$.

delayed with the increase in ω_r which is reflected by the cylinder as well as the pendulum oscillation amplitudes in Figs. 5(a) and (b), respectively.

With the change in ω_r, the natural frequency of the pendulum changes. Therefore, the dominant frequency of oscillation of the cylinder f (which is equal to the vortex shedding frequency) is non-dimensionalized by the pendulum frequency $f_{n,p}$ in this scenario, to understand the parametric synchronization due to NRGP in Fig. 5(c). It can be observed that thus non-dimensionalization collapses the response frequency for the various ω_r along $f/f_{n,p} = 2$. As expected, for $\omega_r = 0.5$, the $f/f_{n,p} = 2$ is equivalent to the VIV synchronization region from $U_r = 4.5 - 8$, and the parametric synchronization does not happen for $U_r \geq 8.5$. For the other cases of $\omega_r = 1$, 1.3 and 1.5, the parametric synchronization occurs at $U_r = 9$, 11 and 12.5, respectively. This corroborated the observations of the response amplitudes of the cylinder and the pendulum. In case of $\omega_r = 0.5$, the drop in the cylinder and pendulum oscillation amplitudes can be associated with the deviation of $f/f_{n,p}$ at $U_r = 17$ to 20.

The piezoelectric characteristics for $\omega_r \in [0.5, 1, 1.3, 1.5]$ and PZH-VIV are presented in Fig. 6. The variation of the root-mean-square of the dimensionless electric

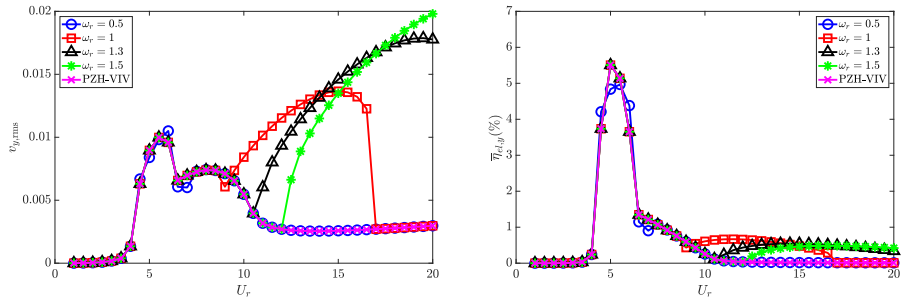

(a) **(b)**

Fig. 6: Effect of ω_r in the introduction of NRGP with U_r on: (a) electric tension $v_{y,\mathrm{rms}}$, and (b) energy harvesting efficiency $\overline{\eta}_{el,y}$. Here, $\overline{m} = 0.3$, $l_d = 0.1$ and $\zeta_\theta = 0.0011$.

tension with the reduced velocity is depicted in Fig. 6(a). In the case of PZH-VIV model, the peak $v_{y,\mathrm{rms}}$ is 0.01 at $U_r = 5.5$. On attaching the pendulum the electric tension increases in the de-synchronized region, which is more prominent with higher values of ω_r. The effect of the NRGP excitation and the delay in it across U_r with increasing ω_r is also translated in the variation of $v_{y,\mathrm{rms}}$. The variation of piezoelectric efficiency with U_r is shown in Fig. 6(b). It has a maximum efficiency of 5.5% in all the cases considered at $U_r = 5$. Addition of pendulum helps in increasing the efficiency to 0.5% for NRGP system in the higher U_r region. It should be noted that the electric tension and efficiency for $\omega_r = 0.5$ is similar to PZH-VIV, as the internal resonance occurs at the VIV region for this condition. Therefore, the efficiency is zero at the de-synchronized region.

4.2 Effect of mass ratio ($\overline{m}$)

The mass ratio ($\overline{m}$) defined as the ratio of the mass of the cylinder to that of the combined cylinder and pendulum system, is another important parameter in the investigation of the response characteristics of NRGP system. The effect of $\overline{m}$ is investigated by keeping the values of $\omega_r = 1.3$, $l_d = 0.1$ and $\zeta_\theta = 0.0011$ fixed and varying $\overline{m} \in [0.1, 0.2, 0.3, 0.5]$.

The response of the cylinder and pendulum oscillations with varying mass ratio is shown in Fig. 7. It can be observed that the change in $y_{\max}$ is small with $\overline{m}$, with the maximum displacement occurring for $\overline{m} = 0.1$ in the de-synchronized region. As the $\overline{m}$ increases, the oscillation amplitude decreases for $10 \leq U_r \leq 18$. Figure 7(b) presents the variation of pendulum displacement with mass ratio. The initiation of the increase in response amplitude for both the cylinder and the pendulum remains at a similar U_r value for various mass ratios. In the de-synchronized region, at a particular U_r, the maximum pendulum oscillation amplitude decreases with increase in $\overline{m}$. The dominant frequency response of the cylinder is shown in Fig. 7(c). The VIV lock-in region is identical for all the mass ratios. The parametric excitation as a result of the attached NRGP is observed from $U_r \geq 11$. As $\omega_r = 1.3$ here, the dominant frequency at the de-synchronized region is $2.6 f_{n,y}$

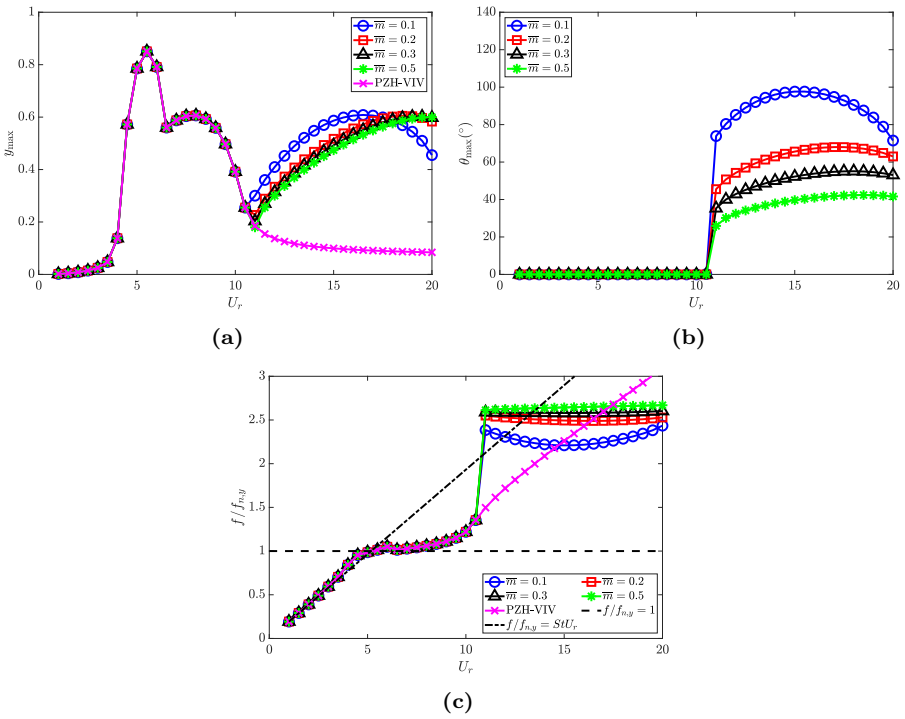

Fig. 7: Response characteristics of the system for various $\overline{m}$ with U_r: (a) maximum non-dimensional oscillation amplitude ($y_{\max}$) of the cylinder, (b) maximum angular rotation of the pendulum $\theta_{\max}$ in degrees ($^\circ$) and (c) dominant frequency with respect to cylinder natural frequency $f/f_{n,y}$. Here, $\omega_r = 1.3$, $l_d = 0.1$ and $\zeta_\theta = 0.0011$.

which translates to $f/f_{n,p} = 2$. A peculiar behavior is observed for $\overline{m} = 0.1$ where the dominant frequency deviates from $f/f_{n,p} = 2$ slightly. Compared to the NRGP model, the PZH-VIV model shows no excitation in the de-synchronized region due to the absence of the pendulum.

Figure 8(a) shows the variation of electric tension with reduced velocity. In case of PZH-VIV, the peak of 0.01 is observed at $U_r = 5.5$. Introduction of the pendulum in the system increases the maximum rms electric tension $v_{y,\text{rms}}$ by about 42%. With increase in $\overline{m}$, the electric tension also increases. The maximum electric tension estimated is 0.0175 for $\overline{m} = 0.5$. The increase of electric tension is attributed to internal resonance in the de-synchronized region. For $\overline{m} = 0.1$, the maximum electric tension is observed at $U_r = 17$, and decreases with increase in U_r. The variation of efficiency with U_r is presented in Fig. 8(b). It has a maximum efficiency of 5.5% for system with NRGP and PZH-VIV cases. Addition of pendulum helps to achieve higher efficiency of 0.5% at $U_r \geq 11$, as shown in the figure. However, the influence of mass ratio on the efficiency is observed to be negligible.

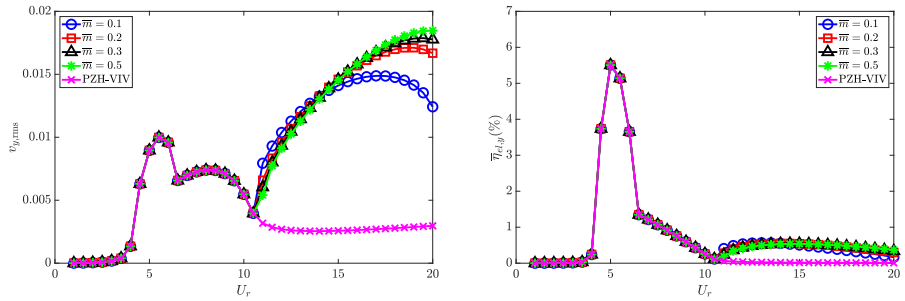

(a) **(b)**

Fig. 8: Effect of $\overline{m}$ in the introduction of NRGP with U_r on: (a) electric tension $v_{y,\mathrm{rms}}$, and (b) energy harvesting efficiency $\overline{\eta}_{el,y}$. Here, $\omega_r = 1.3$, $l_d = 0.1$ and $\zeta_\theta = 0.0011$.

4.3 Effect of torsional damping ratio ζ_θ

The effect of the torsional damping ratio (ζ_θ) for the NRG pendulum on the autoparametric excitation of the cylinder is studied in this sub-section. Four representative values of the damping ratio are considered, viz., $\zeta_\theta \in [2.75\times10^{-4}, 1.1\times10^{-3}, 4.4\times10^{-3}, 1.76\times10^{-2}]$. The other crucial parameters are held constant at $\overline{m} = 0.3$, $l_d = 0.1$ and $\omega_r = 1.3$.

The response characteristics of the cylinder and the pendulum depicting the effects of the damping ratio are shown in Fig. 9. The torsional damping is observed to affect the initiation of the autoparametric excitation. It occurs at $U_r = 10.5$, 11 and 13 for $\zeta_\theta = 2.75\times10^{-4}$, 1.1×10^{-3} and 4.4×10^{-3}, respectively. However, these is no internal resonance observed for the high damping value of $\zeta_\theta = 1.76\times10^{-2}$ and the cylinder response follows the PZH-VIV model (Fig. 9(a)). The maximum oscillation amplitudes for the cylinder and the pendulum also decreases for higher ζ_θ values. The delay in the initiation of internal resonance with respect to U_r as ζ_θ increases is confirmed by the dominant frequency plot in Fig. 9(c). This delay also indicates that the energy extraction window reduces with increase in ζ_θ for the range of U_r considered in the study.

The dimensionless electric tension and the energy harvesting efficiency for varying ζ_θ are shown in Figs. 10(a) and (b), respectively. The electric tension is maximum for lowest torsional damping ratio, i.e., $\zeta_\theta = 2.75\times10^{-4}$ as observed in the internal resonance region. The reduction in the electrical tension is observed with increase in torsional damping. Similar to the cylinder oscillation amplitude, the electric tension of $\zeta_\theta = 1.76\times10^{-2}$ follows the PZH-VIV trend for all the U_r considered in this study. In Fig. 10(b), for lower values of ζ_θ there is a rise in efficiency in the internal resonance region. Maximum efficiency achieved for all four cases is 5.8% at $U_r = 5$ (VIV region) and in the de-synchronized region, the maximum efficiency is about 0.5%. These results are quite intuitive as an increase in the torsional damping will tend to damp out the oscillations of the pendulum leading to negligible effects on the autoparametric excitation. Therefore, the torsional damping is supposed to be kept at a lower value for obtaining the benefits of NRGP autoparametric excitation in the de-synchronized region.

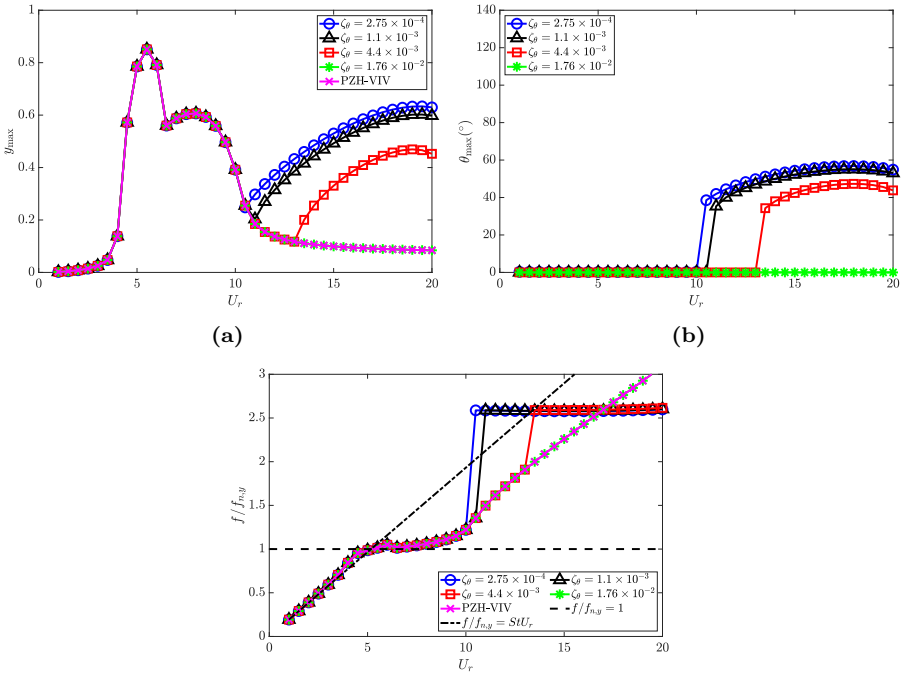

Fig. 9: Response characteristics of the system for various ζ_θ with U_r: (a) maximum non-dimensional oscillation amplitude ($y_{\max}$) of the cylinder, (b) maximum angular rotation of the pendulum $\theta_{\max}$ in degrees ($^\circ$) and (c) dominant frequency with respect to cylinder natural frequency $f/f_{n,y}$. Here, $\overline{m} = 0.3$, $l_d = 0.1$ and $\omega_r = 1.3$.

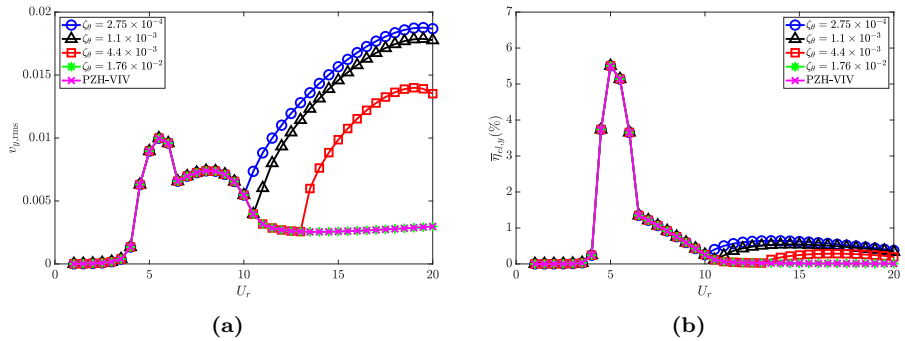

Fig. 10: Effect of ζ_θ in the introduction of NRGP with U_r on: (a) electric tension $v_{y,\mathrm{rms}}$, and (b) energy harvesting efficiency $\overline{\eta}_{el,y}$. Here, $\overline{m} = 0.3$, $l_d = 0.1$ and $\omega_r = 1.3$.

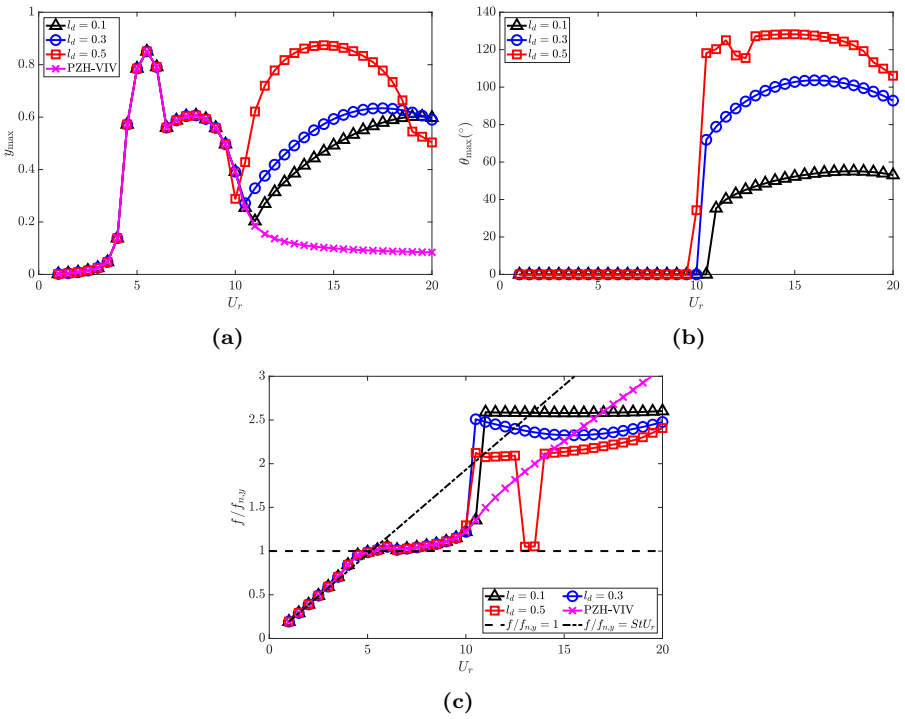

Fig. 11: Response characteristics of the system for various l_d with U_r: (a) maximum non-dimensional oscillation amplitude ($y_{\max}$) of the cylinder, (b) maximum angular rotation of the pendulum $\theta_{\max}$ in degrees ($^\circ$) and (c) dominant frequency with respect to cylinder natural frequency $f/f_{n,y}$. Here, $\overline{m} = 0.3$, $\omega_r = 1.3$ and $\zeta_\theta = 0.0011$.

4.4 Effect of ratio of cylinder diameter to pendulum length l_d

Finally, the effect of the ratio of cylinder diameter D to the length of the pendulum L on the internal resonance of the NRGP-PZH-VIV system is investigated in this sub-section. To accomplish this, we consider $l_d \in [0.1, 0.3, 0.5]$ while keeping the other parameters constant at $\overline{m} = 0.3$, $\omega_r = 1.3$ and $\zeta_\theta = 0.0011$.

The cylinder oscillation amplitude $y_{\max}$ for $l_d = 0.5$ is observed to be maximum compared to other l_d values as shown in Fig. 11(a). The maximum cylinder oscillation achieved in the de-synchronized region is at $U_r = 15$, which is equal to the amplitude estimated at $U_r = 6$. It is worth noting that highest oscillation amplitude achieved in the de-synchronized region is for the NRGP system with $l_d = 0.5$, $\overline{m} = 0.3$, $\omega_r = 1.3$ and $\zeta_\theta = 0.0011$ compared to other parametric investigations discussed earlier. Similar to the cylinder oscillation amplitude, the maximum pendulum oscillation is achieved for $l_d = 0.5$, as shown in the Fig. 11(b). It can be observed that the range of U_r values for getting the autoparametric excitation increases with increase in l_d. The $f/f_{n,y}$ values for $l_d = 0.1$, 0.3 and 0.5 are presented in Fig. 11(c). The $f/f_{n,y}$ increases at $U_r = 11$ till $U_r = 12.5$ for $l_d = 0.5$.

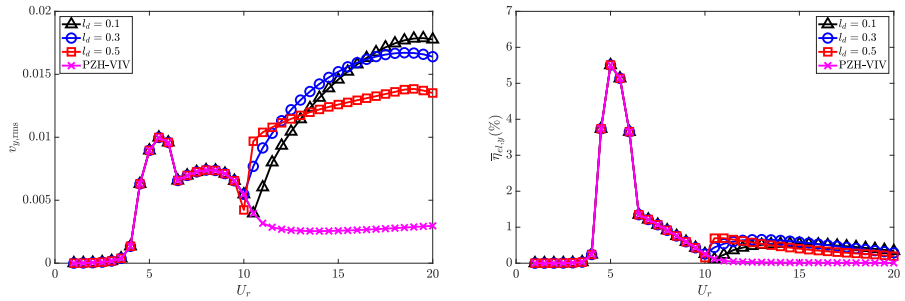

(a) **(b)**

Fig. 12: Effect of l_d in the introduction of NRGP with U_r on: (a) electric tension $v_{y,\mathrm{rms}}$, and (b) energy harvesting efficiency $\overline{\eta}_{el,y}$. Here, $\overline{m} = 0.3$, $\omega_r = 1.3$ and $\zeta_\theta = 0.0011$.

Then the $f/f_{n,y}$ drops at $U_r = 13$ and 13.5 close to the VIV lock-in frequency. The $f/f_{n,y}$ again increases to at $U_r = 14$ till $U_r = 20$. The drop in the $f/f_{n,y}$ values at $U_r = 13$ and 13.5 reflects the lock-in behavior as in the case of synchronized region.

The electric tension and efficiency are presented in Figs. 12(a) and (b), respectively. The maximum electric tension is observed for $l_d = 0.1$ at $U_r = 20$, and it decreases with increase in l_d as shown in Fig. 12(a) at high U_r. As shown in the Fig. 12(b), the efficiency of all the three cases are computed to be 5.5% and 0.5% in the synchronized and de-synchronized regions, respectively.

5 Conclusions

In this work, a VIV based device for electrical energy extraction using piezoelectric harvester is proposed in which a non-linear rotative gravity pendulum (NRGP) is attached. It is observed that the addition of a pendulum to a cylinder undergoing 1-DoF VIV increases the maximum electrical output nearly by four times than a device without the pendulum. A significant increase in the cylinder displacement can be observed for reduced velocity greater than 10, i.e, in the de-synchronized region. This can be attributed to the internal resonance between the cylinder and the pendulum system. The coupled cylinder-pendulum parameters ω_r, $\overline{m}$, ζ_θ and l_d play an important role in the energy harvesting capability of the system. Some of the key findings from the current study are:

- The presence of the non-linear rotative gravity pendulum results in internal resonance of the cylinder-pendulum system at de-synchronized regime ($U_r > 11$) where the cylinder oscillates with a dominant frequency twice of the pendulum natural frequency.
- The onset of the autoparametric excitation gets delayed in terms of U_r with increase in ω_r and ζ_θ. It remains at a similar U_r value for various $\overline{m}$ and gets advanced with increase in l_d.
- The piezoelectric harvesting efficiency is observed to be higher in the de-synchronized region compared to the case without the pendulum.

The modeling of fluid forces can be improved by considering fully coupled incompressible Navier-Stokes equations rather than the wake-oscillator model. Furthermore, experimentation of the NRGP-PZH-VIV model and the possibility of harvesting energy for NRGP-VIV system considering electrostatic/electromagnetic extraction and their comparison can be explored in future research.

Acknowledgements

This work was carried out under the auspices of Early Carrier Research (ECR) Grant from the Science and Engineering Research Board (SERB), Government of India; Grant No: ECR/2018/000687.

Competing Interests

The authors have no relevant financial or non-financial interests to disclose.

Author Contributions

All authors contributed to the study conception and design. Material preparation and analysis were performed by Annette joy, Vaibhav Joshi, Kumar Narendran and Ritwik Ghoshal. The first draft of the manuscript was written by Annette Joy and all authors commented on previous versions of the manuscript. All authors read and approved the final manuscript.

Data Availability

The data that support the findings of this study are available from the corresponding author upon reasonable request.

References

1. Abohamer, M.K., Awrejcewicz, J., Starosta, R., Amer, T.S., Bek, M.A.: Influence of the motion of a spring pendulum on energy-harvesting devices. Applied Sciences **11**(18) (2021). DOI 10.3390/app11188658
2. Arionfard, H., Nishi, Y.: Experimental investigation of a drag assisted vortex-induced vibration energy converter. Journal of Fluids and Structures **68**, 48–57 (2017)
3. Barrero-Gil, A., Alonso, G., Sanz-Andres, A.: Energy harvesting from transverse galloping. Journal of Sound and Vibration **329**(14), 2873–2883 (2010)
4. Bearman, P.W.: Vortex shedding from oscillating bluff bodies. Annual review of fluid mechanics **16**(1), 195–222 (1984)
5. Bernitsas, M.M., Raghavan, K., Ben-Simon, Y., Garcia, E.: Vivace (vortex induced vibration aquatic clean energy): a new concept in generation of clean and renewable energy from fluid flow. In: International Conference on Offshore Mechanics and Arctic Engineering, vol. 47470, pp. 619–637 (2006)
6. Birkhoff, G.: Formation of vortex streets. Journal of Applied Physics **24**(1), 98–103 (1953)
7. Birkhoff, G., et al.: Jets, wakes, and cavities, vol. 2. Elsevier (2012)
8. Blevins, R.D.: Flow-induced vibrations. Van Nostrand Reinhold (1990)

9. Das, S., Wahi, P.: Approximations for period-1 rotation of vertically and horizontally excited parametric pendulum. Nonlinear Dynamics **88**, 2171–2201 (2017)
10. Das, S., Wahi, P.: Energy extraction from vortex-induced vibrations using period-1 rotation of an autoparametric pendulum. Proceedings of the Royal Society A: Mathematical, Physical and Engineering Sciences **474**(2213), 20180086 (2018)
11. Elahi, H., Eugeni, M., Gaudenzi, P.: A review on mechanisms for piezoelectric-based energy harvesters. Energies **11**(7) (2018)
12. Elvin, N.G., Elvin, A.A.: An experimentally validated electromagnetic energy harvester. Journal of Sound and Vibration **330**(10), 2314–2324 (2011)
13. Facchinetti, M.L., De Langre, E., Biolley, F.: Coupling of structure and wake oscillators in vortex-induced vibrations. Journal of Fluids and structures **19**(2), 123–140 (2004)
14. Franzini, G.R.: An elastic rotative nonlinear vibration absorber (ERNVA) as a passive suppressor for vortex-induced vibrations. Nonlinear Dynamics **103**, 255–277 (2021)
15. Franzini, G.R., Bunzel, L.O.: A numerical investigation on piezoelectric energy harvesting from vortex-induced vibrations with one and two degrees of freedom. Journal of Fluids and Structures **77**, 196–212 (2018)
16. Franzini, G.R., Campedelli, G.R., Mazzilli, C.E.N.: A numerical investigation on passive suppression of the parametric instability phenomenon using a rotative non-linear vibration absorber. International Journal of Non-Linear Mechanics **105**, 249–260 (2018)
17. Franzini, G.R., Goncalves, R., Meneghini, J., Fujarra, A.L.: Comparison between force measurements of one and two degrees-of-freedom viv on cylinder with small and large mass ratio. In: Proceedings of the 10th International Conference on Flow-Induced Vibration and Flow-Induced Noise (FIV 2012), 3–6 July 2012, Dublin, p. 561 (2012)
18. Griffin, O.M., Ramberg, S.E.: The vortex-street wakes of vibrating cylinders. Journal of Fluid Mechanics **66**(3), 553–576 (1974)
19. Hamlehdar, M., Kasaeian, A., Reza, M.: Energy harvesting from fluid flow using piezoelectrics: A critical review. Renewable Energy **143**, 1826–1838 (2019)
20. Hartlen, R.T., Currie, I.G.: Lift-oscillator model of vortex-induced vibration. Journal of the Engineering Mechanics Division **96**(5), 577–591 (1970)
21. Jbaily, A., Yeung, R.W.: Piezoelectric devices for ocean energy: a brief survey. Journal of Ocean Engineering and Marine Energy **1**(1), 101–118 (2015)
22. Lallart, M., Richard, C., Garbuio, L., Petit, L., Guyomar, D.: High efficiency, wide load bandwidth piezoelectric energy scavenging by a hybrid nonlinear approach. Sensors and Actuators A: Physical **165**(2), 294–302 (2011)
23. Liu, W., D'Angelo, B.: Mass considerations for viv driven cantilever beam and tethered buoy with internal pendulum. 2014 Oceans - St. John's pp. 1–6 (2014)
24. Marszal, M., Witkowski, B., Jankowski, K., Perlikowski, P., Kapitaniak, T.: Energy harvesting from pendulum oscillations. International Journal of Non-Linear Mechanics **94**, 251–256 (2017)
25. Mehmood, A., Abdelkefi, A., Hajj, M., Nayfeh, A., Akhtar, I., Nuhait, A.: Piezoelectric energy harvesting from vortex-induced vibrations of circular cylinder. Journal of Sound and Vibration **332**(19), 4656–4667 (2013)
26. Narendran, K., Murali, K., Sundar, V.: Investigations into efficiency of vortex induced vibration hydro-kinetic energy device. Energy **109**, 224–235 (2016)
27. Nishi, Y., Fukuda, K., Shinohara, W.: Experimental energy harvesting from fluid flow by using two vibrating masses. Journal of Sound and Vibration **394**, 321–332 (2017)
28. Ogink, R., Metrikine, A.: A wake oscillator with frequency dependent coupling for the modeling of vortex-induced vibration. Journal of Sound and Vibration **329**(26), 5452–5473 (2010)
29. Roshko, A.: Experiments on the flow past a circular cylinder at very high reynolds number. Journal of fluid mechanics **10**(3), 345–356 (1961)
30. Sarpkaya, T.: A critical review of the intrinsic nature of vortex-induced vibrations. Journal of fluids and structures **19**(4), 389–447 (2004)
31. Skop, R., Griffin, O.: A model for the vortex-excited resonant response of bluff cylinders. Journal of Sound and Vibration **27**(2), 225–233 (1973)
32. Song, R., Shan, X., Lv, F., Li, J., Xie, T.: A novel piezoelectric energy harvester using the macro fiber composite cantilever with a bicylinder in water. Applied Sciences **5**(4), 1942–1954 (2015)
33. Soti, A.K., Thompson, M.C., Sheridan, J., Bhardwaj, R.: Harnessing electrical power from vortex-induced vibration of a circular cylinder. Journal of Fluids and Structures **70**, 360–373 (2017)

34. Sumer, B.M., Fredsøe, J.: Hydrodynamics around cylindrical strucures, vol. 26. World scientific (2006)
35. Truitt, A.: Enery harvesting through wind excitation of a piezoelectric flag-like harvester. Ph.D. thesis, University of Alabama Libraries (2013)
36. Ueno, T., Franzini, G.R.: Numerical studies on passive suppression of one and two degrees-of-freedom vortex-induced vibrations using a rotative non-linear vibration absorber. International Journal of Non-Linear Mechanics **116**, 230–249 (2019)
37. Wang, D.A., Ko, H.H.: Piezoelectric energy harvesting from flow-induced vibration. Journal of Micromechanics and Microengineering **20**(2), 025019 (2010)
38. Williamson, C.H., Govardhan, R.: Vortex-induced vibrations. Annu. Rev. Fluid Mech. **36**, 413–455 (2004)